Scientia Iranica B (2012) 19 (4), 1053–1065

Sharif University of Technology

Scientia Iranica

Transactions B: Mechanical Engineering

www.sciencedirect.com

Lattice Boltzmann simulation of MHD mixed convection in a lid-driven square cavity with linearly heated wall

GH.R. Kefayati *, **M. Gorji-Bandpy**, **H. Sajjadi**, **D.D. Ganji**

Department of Mechanical Engineering, Babol University of Technology, Babol, Mazandaran, P.O. Box 484, Iran

Received 9 May 2011; revised 12 April 2012; accepted 15 May 2012

KEYWORDS

Mixed convection;
Magnetohydrodynamic (MHD);
Hartmann number;
Lattice Boltzmann method;
Heat transfer.

Abstract Solving of MHD flow by the lattice Boltzmann method, utilizing classical equations has been investigated by presenting MHD mixed convection in a lid-driven cavity by a linearly heated wall. The Hartmann number varied from Ha = 0 to 100; furthermore, the study has been conducted for Richardson numbers (Ri) from 0.01 to 100, while the directions of the magnetic field were investigated for $\theta = 0^\circ$ and 90°. Results show that the augmentation of Richardson number causes heat transfer to increase, as the heat transfer decreases by the increment of Hartmann number for various Richardson numbers and the directions of the magnetic field. The highest decline of heat transfer on the linearly heated wall was found at $\theta = 0^\circ$ for Richardson numbers of Ri = 100 and Ha = 100. On the other hand, the least effect of the magnetic field is observed at Ri = 0.01 from Ha = 25 to 100 for both directions on the linearly heated wall. Moreover, the magnetic field influences heat transfer marginally at $\theta = 90^\circ$ against $\theta = 0^\circ$, which changes dramatically. Heat transfer on the heated wall at the bottom of the cavity behaves like the linearly heated wall regarding the effect of the magnetic field.

1. Introduction

Flow and heat transfer analysis in lid-driven cavities is one of the most widely studied problems in thermo-fluids areas. Numerous investigations have been conducted in the past on lid-driven cavity flow and heat transfer, considering various combinations of imposed temperature gradients and cavity configurations [1–8]. This is because the driven cavity configuration is encountered in many practical engineering and industrial applications, such as materials processing, flow and heat transfer in solar ponds, dynamics of lakes, reservoirs and cooling ponds, crystal growing, float glass production, metal casting, food processing, galvanizing, metal coating and so on.

The flow of an electrically conducting fluid in a magnetic field is influenced by magnetohydrodynamic (MHD) forces resulting from the interaction of induced electric currents with the applied magnetic field. An externally imposed magnetic field is also a widely used tool for control of melt flows in the bulk crystal growth of semiconductors. One of the main purposes of electromagnetic control is to stabilize the flow and suppress oscillatory instabilities, which degrades the resulting crystal. Wide ranges of investigations were conducted by researchers in MHD natural convection. Kahveci and Oztuna [9] investigated MHD natural convection flow and heat transfer in a laterally heated partitioned enclosure. They showed that the *x*-directional magnetic field is more effective in damping convection than the *y*-directional magnetic field, and the average heat transfer rate decreases with an increase in the distance of the partition from the hot wall. Also, they demonstrated that the average heat transfer rate decreases up to 80% if the partition is placed at the midpoint and an *x*-directional magnetic, and that flow and heat transfer have little dependence on Prandtl number. Pirmohammadi and Ghassemi [10] studied the effect of a magnetic field on convection heat transfer inside a tilted square enclosure. They found that for a given inclination angle (φ), as the value of

* Corresponding author. Tel.: +98 1113234205; fax: +98 1113212268.
E-mail addresses: gholamrezakefayati@gmail.com, gh.rkefayati@yahoo.com (GH.R. Kefayati).

Peer review under responsibility of Sharif University of Technology.

Production and hosting by Elsevier

1026-3098 © 2012 Sharif University of Technology. Production and hosting by Elsevier B.V. Open access under CC BY-NC-ND license.
doi:10.1016/j.scient.2012.06.015

Nomenclature

B	Magnetic field
c	Lattice speed
c_i	Discrete particle speeds
c_p	Specific heat at constant pressure
F	External forces
f	Density distribution functions
f^{eq}	Equilibrium density distribution functions
g	Internal energy distribution functions
g^{eq}	Equilibrium internal energy distribution functions
g_y	Gravity
Gr	Grashof number $\left(\mathrm{Gr} = \frac{\beta g_y H^3 (T_H - T_C)}{\nu^2}\right)$
Ha	Hartmann number $\left(\mathrm{Ha}^2 = \frac{B^2 L^2 \sigma_e}{\mu}\right)$
M	Lattice number
Ma	Mach number
Nu	Nusselt number
Pr	Prandtl number
R	Constant of the gases
Ra	Rayleigh number $\left(\mathrm{Ra} = \frac{\beta g_y H^3 (T_H - T_C)}{\nu \alpha}\right)$
Ri	Richardson number $\left(\mathrm{Ri} = \frac{\mathrm{Gr}}{\mathrm{Re}^2}\right)$
T	Temperature
x, y	Cartesian coordinates
u	Magnitude of velocity at x-direction
v	Magnitude of velocity at y-direction

Greek letters

ω_i	Weighted factor indirection i
β	Thermal expansion coefficient
τ_c	Relaxation time for temperature
τ_v	Relaxation time for flow
ν	Kinematic viscosity
Δx	Lattice spacing
Δt	Time increment
α	Thermal diffusivity
σ	Surface tension

Subscripts

avg	Average
C	Cold
H	Hot
n	Natural convection
B	Magnetic field

Hartmann number (Ha) increases, the convection heat transfer reduces. Furthermore, they obtained that at $\mathrm{Ra} = 10^4$, the value of Nusselt number depends strongly upon the inclination angle for relatively small values of Hartmann number, and at $\mathrm{Ra} = 10^5$, the Nusselt number increases up to about $\varphi = 45^\circ$ and then decrease as φ increases.

Sathiyamoorthy and Chamkha [11] have done a numerical study for the natural convection flow of electrically conducting liquid gallium in a square cavity, where the bottom wall is uniformly heated and the left and right vertical wall are linearly heated, while the top wall is kept thermally insulated. They exhibited that the magnetic field with an inclined angle has effects on the flow and heat transfer rates in the cavity. The number of researchers investigating the effects of MHD mixed convection in lid-driven cavities is very limited. Sivasankaran et al. [12] investigated mixed convection in a square cavity of sinusoidal boundary temperatures at sidewalls in the presence of a magnetic field, numerically. They found that the heat transfer rate increases with the phase deviation up to $\varphi = \pi/2$, and then it decreases for further augmentation in the phase deviation. Then, it was obtained that the heat transfer rate increases on increasing the amplitude ratio. Rahman et al. [13] studied the development of a magnetic field effect on mixed convective flow in a horizontal channel with a bottom heated open enclosure. Their results indicate that various Hartmann, Rayleigh and Reynolds numbers strongly affect the flow phenomenon and temperature field inside the cavity, whereas in the channel, these effects are less significant. Oztop et al. [14] studied mixed convection heat transfer characteristics for a lid-driven air flow within a square enclosure having a circular body. The authors found that the circular body has a significant effect on flow field and temperature distribution. Moreover, Oztop et al. [15] considered Laminar mixed convection flow in the presence of a magnetic field in a top sided lid-driven cavity heated by a corner heater. They exhibited that heat transfer decreases, with increasing of Hartmann number. Nasrin and Parvin [16] conducted a numerical work on the Hydromagnetic effect on mixed convection in a lid-driven cavity with a sinusoidal corrugated bottom surface. They indicated that the average Nusselt number (Nu) at the heated surface increases with a rise in the number of waves, as well as Reynolds number, while decreasing with an increment in Hartmann number.

For more than one decade, the Lattice Boltzmann Method (LBM) has been demonstrated to be a very effective numerical tool for a broad variety of complex fluid flow phenomena that are problematic for conventional methods [17–21]. The kinetic nature of the LBM distinguishes it from other numerical methods, mainly in three aspects. First, the convection operator of the LBM is linear in velocity space, so computational efforts are greatly reduced compared to those of some macroscopic CFD methods, such as the Navier–Stokes equation solvers. Second, the pressure of the LBM can be directly calculated using an equation of state, unlike the direct numerical simulation of the incompressible Navier–Stokes equations in which the pressure must be obtained from the Poisson equation. Third, the LBM utilizes a minimal set of velocities in phase space: therefore, the transformation relating the microscopic distribution function and macroscopic quantities is greatly simplified. The main aim of the present study is to demonstrate the use of the Lattice Boltzmann Method for MHD with a simple and clear statement, and also solving MHD mixed convection as a linearly heated side. Richardson number varies in a wide range from 0.01 to 100. The results of LBM are validated with previous numerical investigations. Effects of Richardson number, Hartman number and various directions of the magnetic field on flow field and temperature distribution are considered simultaneously.

2. Mathematical formulation

2.1. Problem statement

Plotting of the considered model is shown in Figure 1. It is a two-dimensional enclosure with different heated walls. The left vertical is heated linearly and the right vertical wall is kept at a low temperature (T_c). The top horizontal wall has been considered adiabatic, as it was driven with a constant

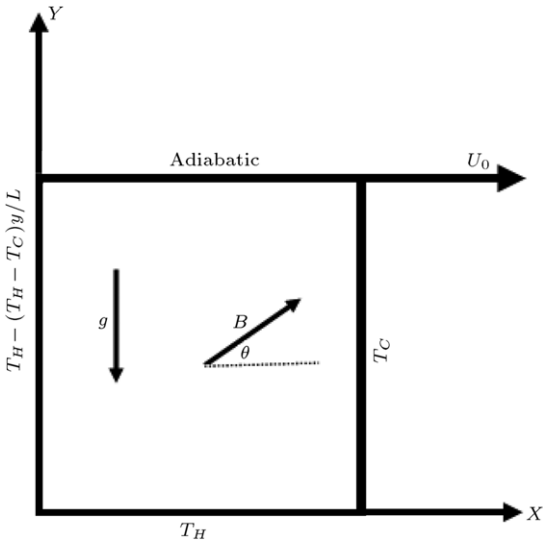

Figure 1: Geometry of the present study.

speed of U_0, and the bottom horizontal wall is maintained at a high temperature (T_H). The cavity is filled with air at a Prandtl number of 0.71. The gravitational acceleration acts downward. The uniform magnetic field, with a constant magnitude (B_0), is applied in the X and Y directions. It is assumed that the induced magnetic field produced by the motion of an electrically conducting fluid is negligible compared to the applied magnetic field. The density varies, while the Boussinesq approximation is valid. The flow is two-dimensional, laminar and incompressible. In addition, it is assumed that the viscous dissipation and Joule heating are neglected.

3. The classic equations for MHD natural convection

The continuity equation (1), the momentum equations (2) and (3) and the energy equation (4) for MHD natural convection by macroscopic variables are written as:

$$\frac{\partial u}{\partial x}+\frac{\partial v}{\partial y}=0, \tag{1}$$

$$\rho\left(u\frac{\partial u}{\partial x}+v\frac{\partial u}{\partial y}\right)=-\frac{\partial p}{\partial x}+\mu\left(\frac{\partial^2 u}{\partial x^2}+\frac{\partial^2 u}{\partial y^2}\right)+F_x, \tag{2}$$

$$\rho\left(u\frac{\partial v}{\partial x}+v\frac{\partial v}{\partial y}\right)=-\frac{\partial p}{\partial y}+\mu\left(\frac{\partial^2 v}{\partial x^2}+\frac{\partial^2 v}{\partial y^2}\right)+F_y, \tag{3}$$

$$u\frac{\partial T}{\partial x}+v\frac{\partial T}{\partial y}=\alpha\left(\frac{\partial^2 T}{\partial x^2}+\frac{\partial^2 T}{\partial y^2}\right), \tag{4}$$

where F_x and F_y are the total body forces in X and Y directions, respectively, and they are defined as follows:

$$F_x=\frac{\mathrm{Ha}^2\mu}{L^2}\left(v\sin\varphi\cos\varphi-u\sin^2\varphi\right), \tag{5}$$

$$F_y=\rho g\beta(T-T_c)+\frac{\mathrm{Ha}^2\mu}{L^2}\left(u\sin\varphi\cos\varphi-v\cos^2\varphi\right), \tag{6}$$

where Ha is Ha $=LB\sqrt{\frac{\sigma}{\mu}}$ as σ is electrical conductivity, B is the magnitude of the magnetic field, L is the length of the cavity and ϕ is the direction of the magnetic field.

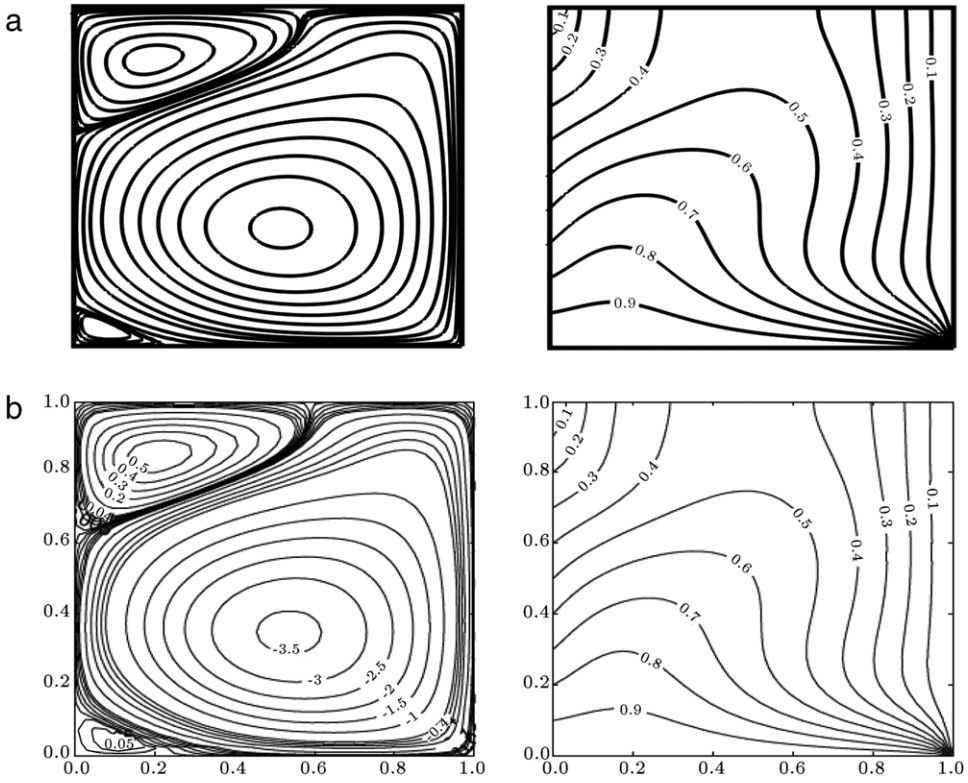

Figure 2: Comparison of the streamlines and isotherms for natural convection at Ra $=10^5$ and Ha $=50$ between (a) the present results and (b) numerical results by Sathiyamoorthy and Chamkha [11].

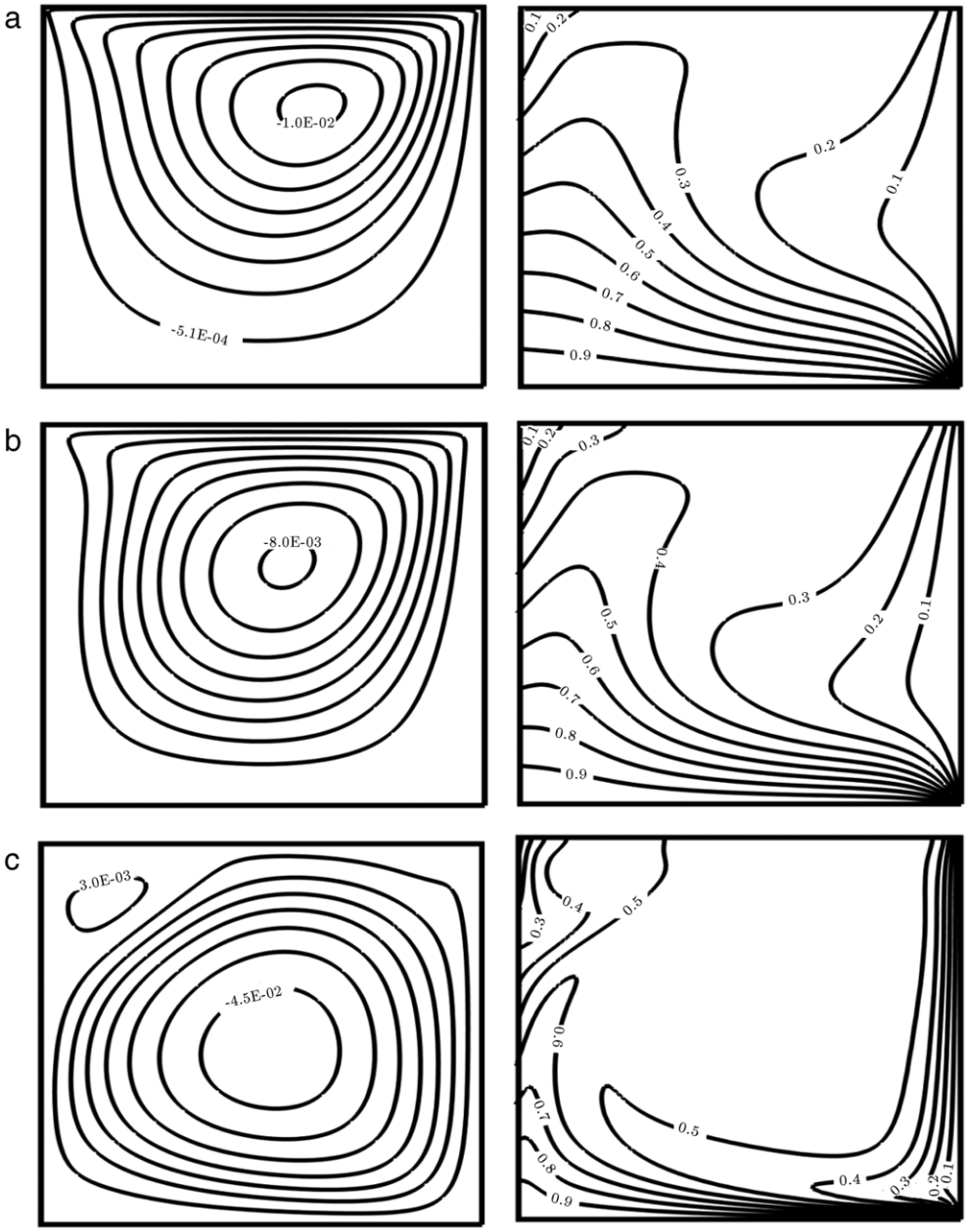

Figure 3: Comparison of the streamlines and isotherms at various Richardson numbers for Ha = 0. (a) Ri = 0.01, (b) Ri = 1, and (c) Ri = 100.

4. Simulation of MHD with the lattice Boltzmann method

4.1. Brief introduction to LBM

The LBM method with standard, two dimensional, nine velocities (D2Q9) for flow and temperature are used in this work; for completeness, only a brief discussion is given in the following paragraphs.

The Lattice Boltzmann equation with external forces can be written as:

For the flow field:

$$f_i(x + c_i\Delta t, t + \Delta t) - f_i(x, t) = -\frac{1}{\tau_v}\left[f_i(x, t) - f_i^{eq}(x, t)\right] + \Delta t F. \quad (7)$$

For the temperature field:

$$g_i(x + c_i\Delta t, t + \Delta t) - g_i(x, t) = -\frac{1}{\tau_c}\left[g_i(x, t) - g_i^{eq}(x, t)\right]. \quad (8)$$

Eq. (7) recovers the continuity and momentum Eqs. (1)–(3), where the total body forces was considered by the external force of Eq. (7). Eq. (8) describes the evolution of the internal energy and leads to Eq. (4).

u and ρ are the macroscopic velocity and density, respectively, c is the lattice speed and is equal to $\Delta x/\Delta y$, where Δx is the lattice space and, similar to the lattice time step, is equal to unity. ω_i is the weighting factor.

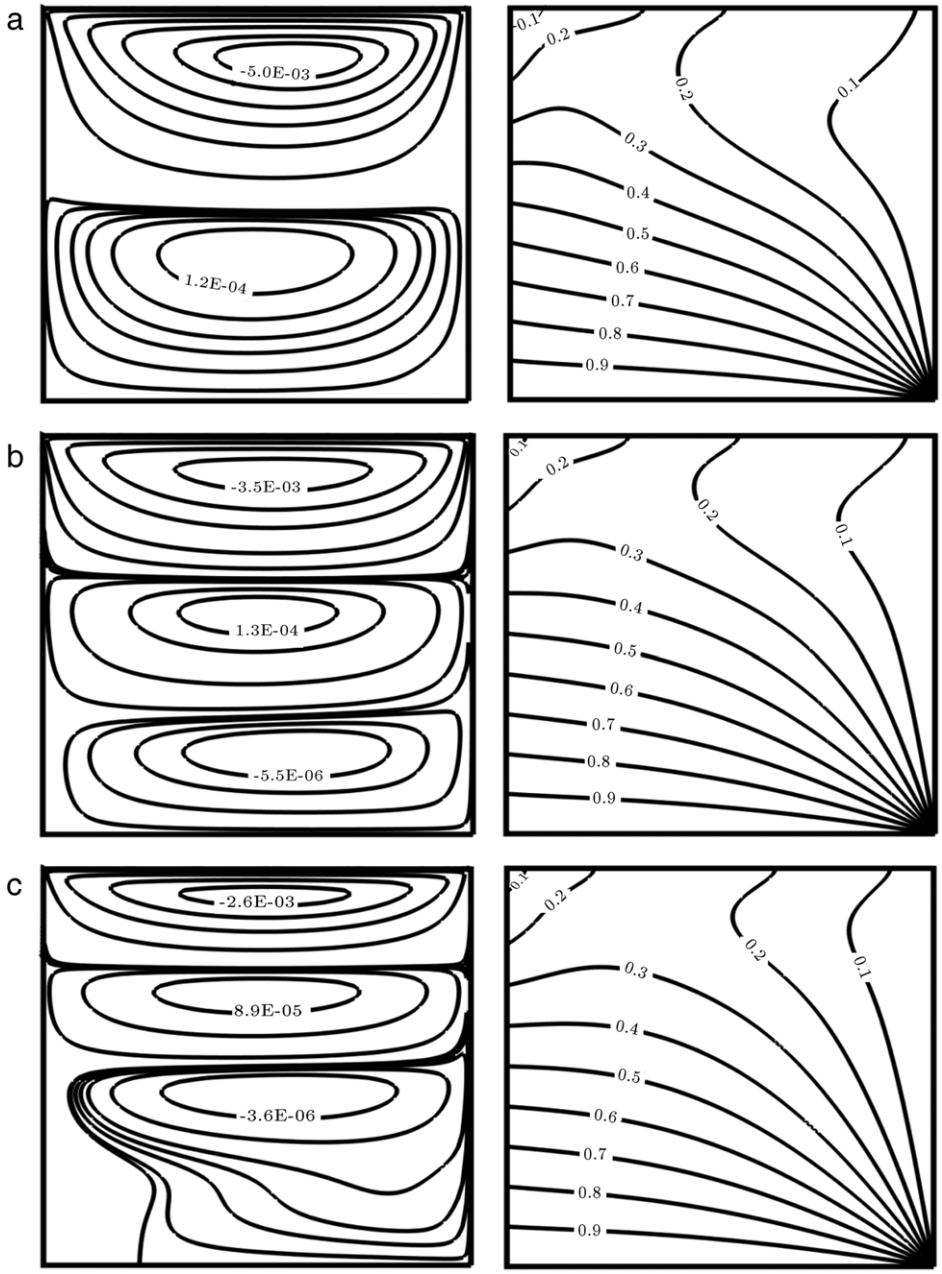

Figure 4: Comparison of the streamlines and isotherms at various Hartman numbers for Ri = 0.01 and $\theta = 0^{\circ}$. (a) Ha = 25, (b) Ha = 50, and (c) Ha = 100.

The D2Q9 model for flow and temperature is used in this work, so the weighting factors and the discrete particle velocity vectors are different for these two models, and they are calculated as follows:

$$f_i^{eq}(x,t) = \omega_i \rho \left[1 + \frac{c_i \cdot u}{c_s^2} + \frac{1}{2}\frac{(c_i \cdot u)^2}{c_s^4} - \frac{1}{2}\frac{u \cdot u}{c_s^2}\right], \tag{9}$$

$$g_i^{eq} = \omega_i T \left[1 + \frac{c_i \cdot u}{c_s^2}\right]. \tag{10}$$

For D2Q9:

$$\omega_i = \begin{cases} 4/9 & i = 0 \\ 1/9 & i = 1-4 \\ 1/36 & i = 5-8. \end{cases} \tag{11}$$

The discrete velocities, c_i, for the D2Q9 (Figure 2a) are defined as follows:

$$c_i = \begin{cases} 0 & i = 0 \\ c\left(\cos\left[(i-1)\frac{\pi}{2}\right], \sin\left[(i-1)\frac{\pi}{2}\right]\right) & i = 1-4 \\ c\sqrt{2}\left(\cos\left[(i-5)\frac{\pi}{2} + \frac{\pi}{4}\right], \sin\left[(i-5)\frac{\pi}{2} + \frac{\pi}{4}\right]\right) & i = 5-8. \end{cases} \tag{12}$$

The kinematic viscosity (ϑ) and the thermal diffusivity (α) are then related to the relaxation times by:

$$\vartheta = \left[\tau_v - \frac{1}{2}\right] c_s^2 \Delta t, \qquad \alpha = \left[\tau_c - \frac{1}{2}\right] c_s^2 \Delta t. \tag{13}$$

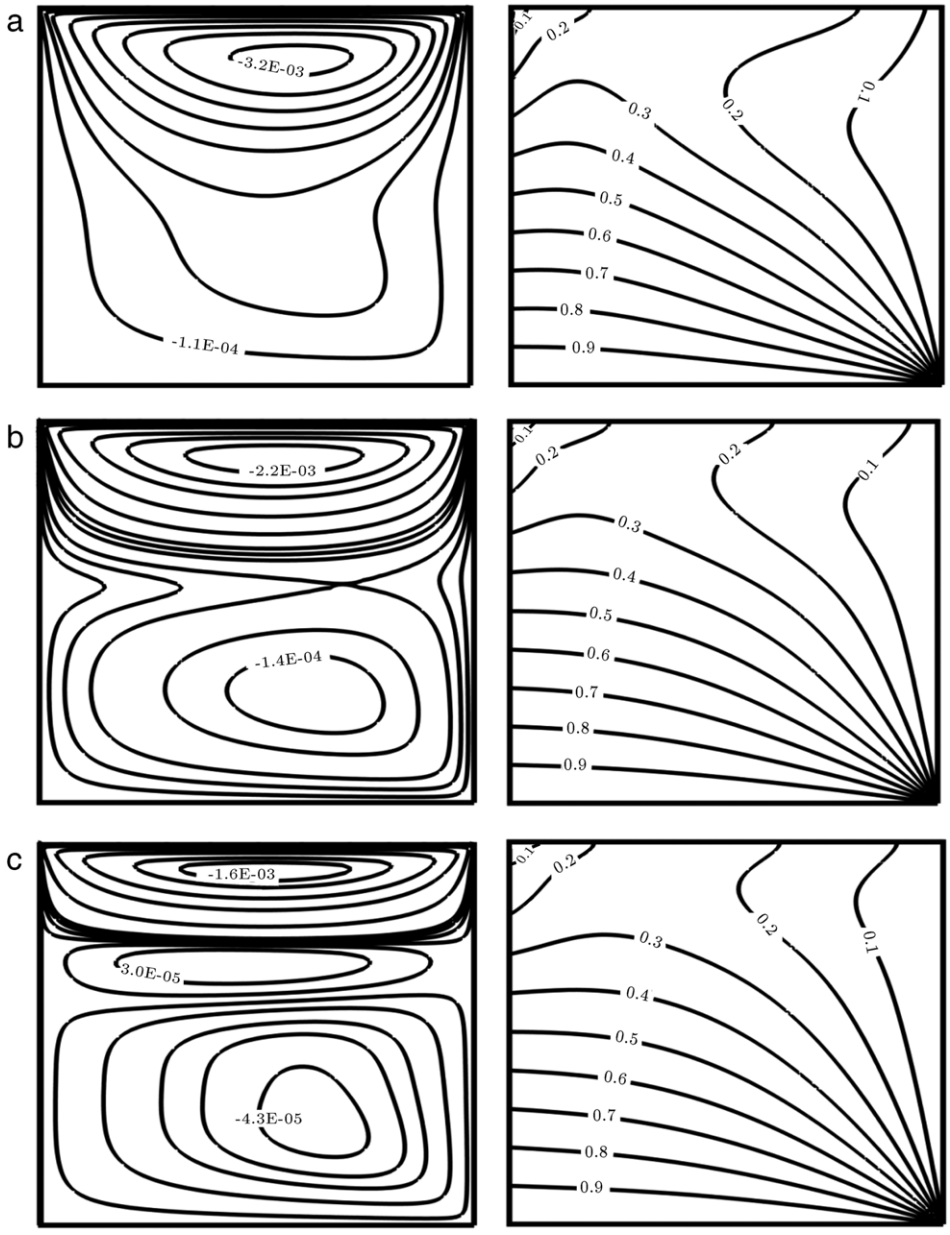

Figure 5: Comparison of the streamlines and isotherms at various Hartman numbers for Ri = 1 and $\theta = 0^{\circ}$. (a) Ha = 25, (b) Ha = 50, and (c) Ha = 100.

Also, the external force appears for LBM as follows:

$$F_i = \omega_i \cdot F \cdot c_i / c_s^2. \tag{14}$$

Because of $c_s = c/\sqrt{3}$, Eq. (12) is written as:

$$F_i = 3 \cdot \omega_i \cdot F. \tag{15}$$

Finally, the macroscopic variable can be calculated in terms of these variables, with the following formula:

Flow density:

$$\rho(x, t) = \sum_i f_i(x, t). \tag{16}$$

Momentum:

$$\rho u(x, t) = \sum_i f_i(x, t) c_i + F. \tag{17}$$

Temperature:

$$T = \sum_i g_i(x, t). \tag{18}$$

4.2. Effect of the magneto field on force term

The effect of the magnetic field was shown only at the force term, where the total body forces at Eqs. (2) and (3) are replaced with the external force at Eq. (7). It should be mentioned that all variables must become dimensionless in the force term of LBM.

$$F = F_x + F_y, \tag{19}$$

$$F_x = 3\omega_k \rho \left(A \left(v \sin(\theta) \cos(\theta)\right) - \left(u \sin^2(\theta)\right)\right), \tag{20}$$

$$F_y = 3\omega_k \rho \big((g\beta \left(T - T_m\right)) + \left(A \left(u \sin(\theta) \cos(\theta)\right) - \left(v \cos^2(\theta)\right)\right)\big), \tag{21}$$

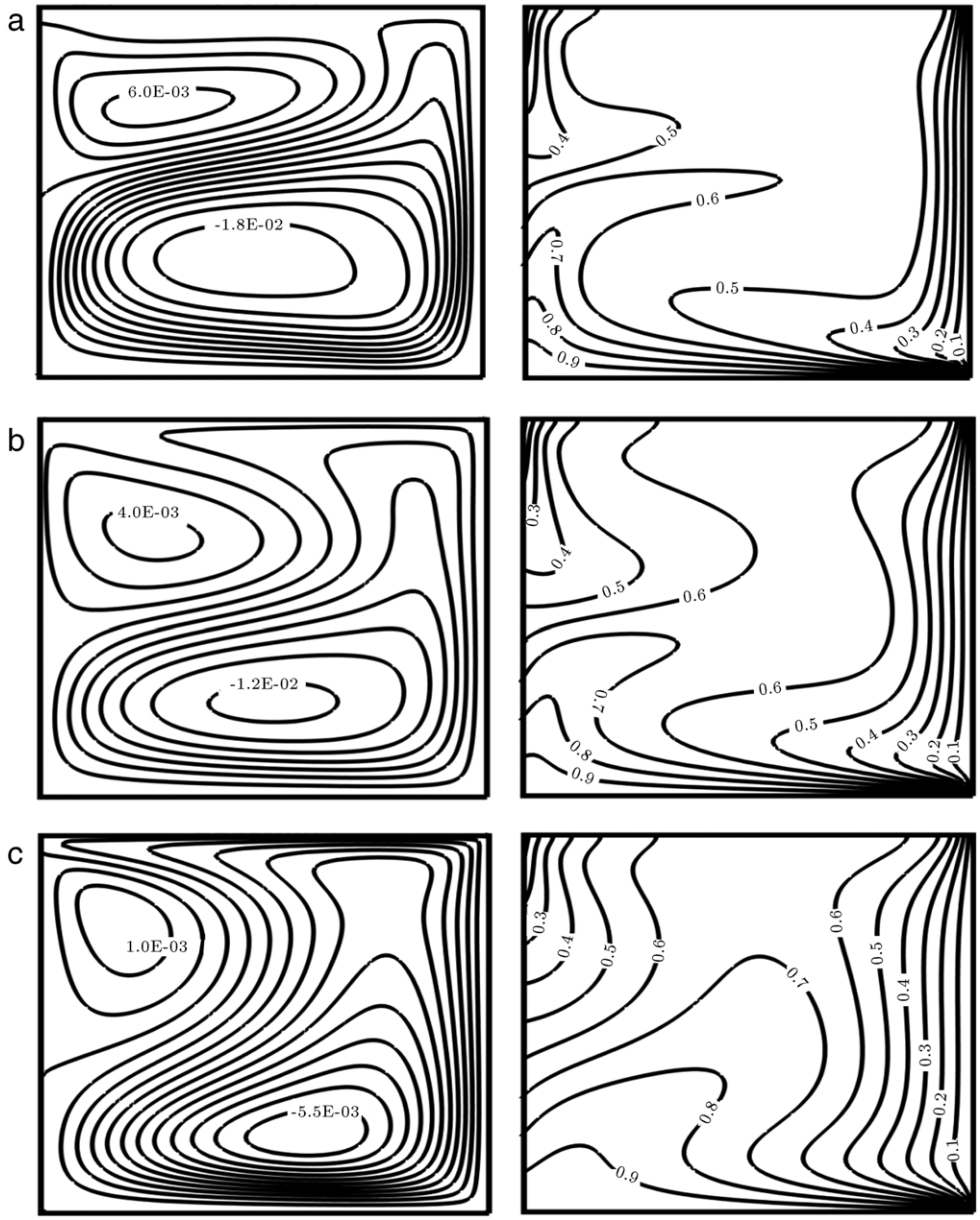

Figure 6: Comparison of the streamlines and isotherms at various Hartman numbers for Ri = 100 and $\theta = 0^{\circ}$. (a) Ha = 25, (b) Ha = 50, and (c) Ha = 100.

where A is defined by:

$$A = \left(\mathrm{Ha}^2\right)\left(\frac{\nu}{M^2}\right). \tag{22}$$

It is clear that (ρA) term at Eqs. (18) and (19) is equal to $\frac{\mathrm{Ha}^2\mu}{L^2}$ at Eqs. (5) and (6), and it just becomes dimensionless.

4.3. Boundary conditions

4.3.1. Flow

Bounce-back boundary conditions were applied on all solid boundaries, which mean that incoming boundary populations are equal to out-going populations after the collision. For instance, for the east boundary, the following conditions are imposed:

$$f_{6,n} = f_{8,n}, \qquad f_{7,n} = f_{5,n}, \qquad f_{3,n} = f_{1,n}, \tag{23}$$

where n is the lattice on the boundary.

4.3.2. Temperature

The bounce back boundary condition (adiabatic) is used on the north of the boundaries. Paradigmatically, for the north boundary, the following conditions are imposed:

$$g_{7,n} = g_{5,n}, \qquad g_{8,n} = g_{6,n}, \qquad g_{4,n} = g_{2,n}. \tag{24}$$

Temperature at the west, east and bottom walls are known in the west wall, $T_H(y) = T_H - (T_H - T_C)y/L$. Since we are using D2Q9, the unknowns are g_1, g_5, g_8, which are evaluated as;

$$g_1 = T_H(y)(\omega_1 + \omega_3) - g_3, \tag{25a}$$

$$g_5 = T_H(y)(\omega_5 + \omega_7) - g_7, \tag{25b}$$

$$g_8 = T_H(y)(\omega_8 + \omega_6) - g_6. \tag{25c}$$

4.4. Method of mixed convection solution

Viscosity is selected to insure that the Mach number is within the limit of incompressible flow (Ma $<$ 0.3). For the

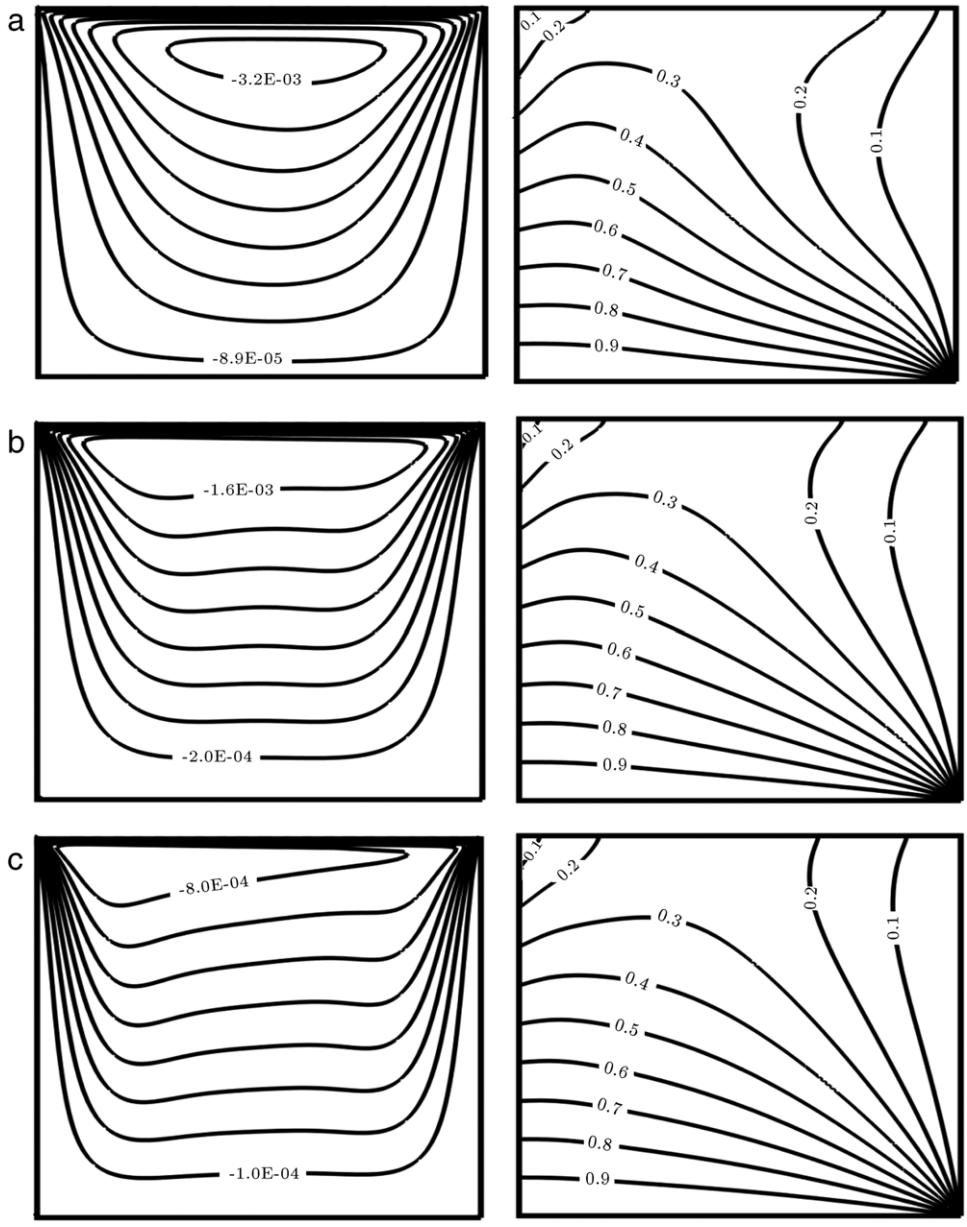

Figure 7: Comparison of the streamlines and isotherms at various Hartman numbers for Ri = 0.01 and $\theta = 90^{\circ}$. (a) Ha = 25, (b) Ha = 50, and (c) Ha = 100.

buoyant flow, by fixing Reynolds number, Prandtl number and Mach number, the viscosity and thermal diffusivity are calculated from their fixed definition:

$$\nu = \frac{1}{\sqrt{\mathrm{Gr}}}\mathrm{Ma}Mc, \tag{26}$$

where M is the number of lattices in the y-direction (parallel to gravitational acceleration). Grashof and Prandtl numbers are defined as $\mathrm{Gr} = \frac{\beta g_y H^3 (T_H - T_C)}{\nu^2}$, and $\mathrm{Pr} = \frac{\nu}{\alpha}$, respectively. In addition, the speed of the lattice is constant ($c = \frac{1}{\sqrt{3}}$). Furthermore, the Mach number is fixed at 0.1 in all computations.

Moreover, the Richardson number ($\mathrm{Ri} = \mathrm{Gr}/\mathrm{Re}^2$) is constant at three values of 0.01,1 and 100.

For getting the speed of the lid-driven side, the following conditions are imposed.

$$u = \frac{\mathrm{Re}\nu}{M}. \tag{27}$$

Eq. (13) are used to calculate the relaxation times for density and temperature distribution functions.

Nusselt number, Nu, is one of the most important dimensionless parameters in describing the convective heat transport. The local Nusselt number and the average value at the hot and cold walls are calculated as:

$$\mathrm{NU}_y = -\frac{L}{\Delta T}\frac{\partial T}{\partial x}, \tag{28}$$

$$\mathrm{NU}_{avg} = \frac{1}{L}\int_0^L \mathrm{NU}_y dy. \tag{29}$$

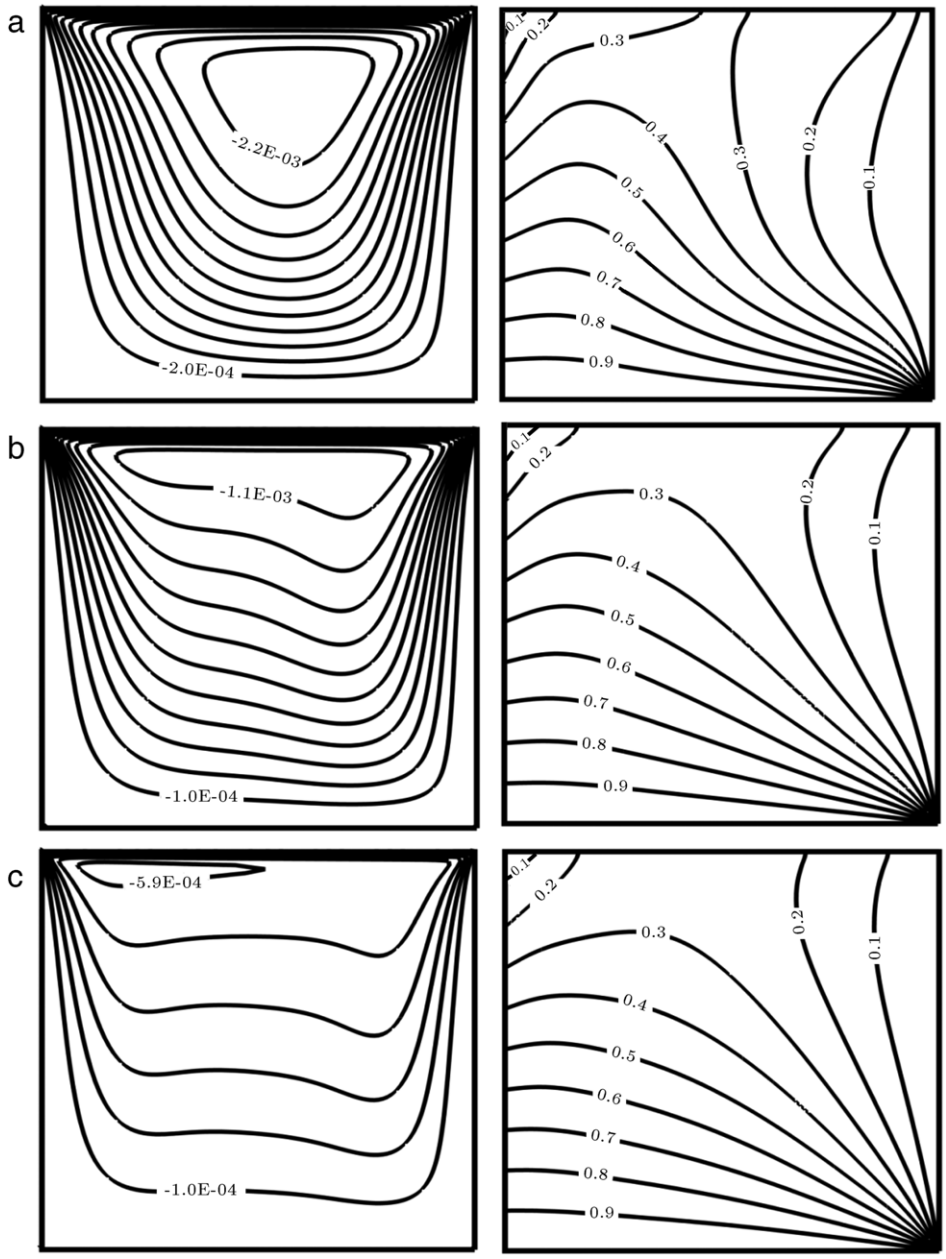

Figure 8: Comparison of the streamlines and isotherms at various Hartman numbers for Ri = 1 and $\theta = 90^{\circ}$. (a) Ha = 25, (b) Ha = 50 and (c) Ha = 100.

Finally, the following criterion to check for the steady-state solution was used:

$$\text{Error} = \max \left|T^{n+1} - T^{n}\right| \leq 10^{-5}. \tag{30}$$

5. Results and discussion

5.1. Code validation and grid independence

This problem was investigated at a fixed Reynolds number of (Re = 100) and various Richardson numbers of ($0.01 <$ Ri < 100), while the Hartmann number changes between 0 and 100, and was considered in X and Y directions. The lattice Boltzmann method scheme was used for obtaining the numerical simulations in a cavity filled with air at Pr = 0.71. A linearly heated boundary was considered. Meanwhile, an extensive mesh testing procedure was examined to guarantee a grid independent solution. Five different mesh combinations and their times were explored for the case of Ri = 1 and Ha = 0. The present code was tested for grid independence by calculating the average Nusselt number on the left wall. In harmony with this, it was found that a grid size of 101_101 ensures a grid independent solution. It was confirmed that the grid size of (101_101) ensures a grid independent solution, as portrayed by Table 1. To check the accuracy of the present results, the present code is validated against published works in the literature on convective flow in lid-driven cavities. The results are compared in Table 2. Moreover, for testing MHD simulation accuracy, as the cavity has a linearly heated side, we compared the present results against the

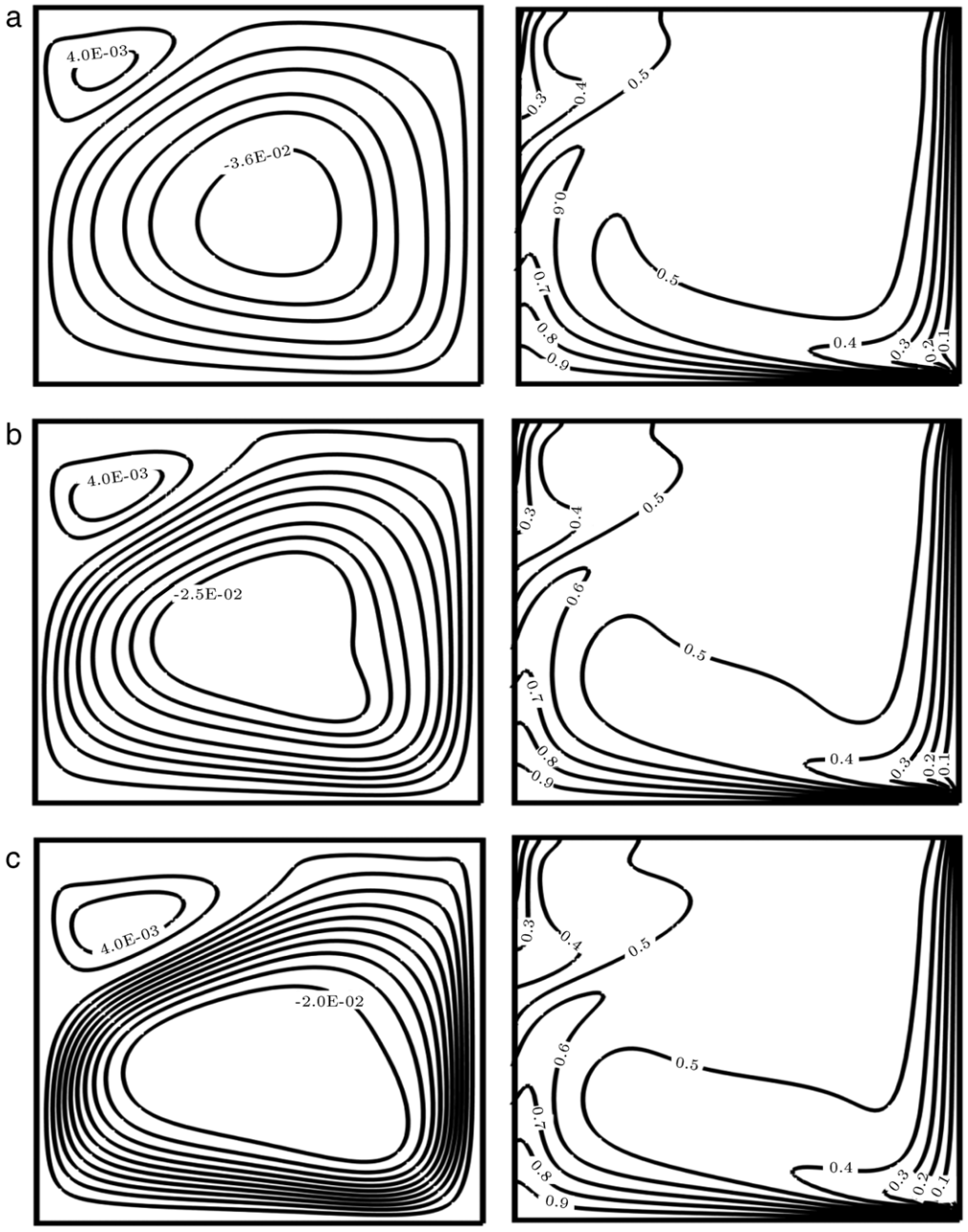

Figure 9: Comparison of the streamlines and isotherms at various Hartman numbers for Ri = 100 and $\theta = 90^{\circ}$. (a) Ha = 25, (b) Ha = 50 and (c) Ha = 100.

work of Sathiyamoorthy and Chamkha [11] (Figure 2). The consequences of this comparison demonstrate the appropriate ability of this method for solving MHD problems.

5.2. Effect of Richardson number on streamlines and isotherms

Figure 3 shows the isotherms and streamlines for various Richardson numbers at Ha = 0. As the Richardson number augments, the isotherms near the walls and the gradient of temperature at heated and linearly heated walls increase. This phenomenon is due to Grashof number enhancement by the increment of Richardson number, provoking heat convection to rise. In addition, the streamlines alter their characteristics from concentration at the top of the cavity in the direction of the lid-driven velocity to a central form, with a secondary circulation created at the top left corner of the cavity at Ri = 100, circulating opposite the main flow in a counterclockwise rotation.

5.3. Effect of Hartmann number on streamlines and isotherms in an X-direction magnetic field

Figure 4 displays the streamlines and the isotherms for different Hartmann numbers at Ri = 0.01. The effect of Hartmann number on the isotherms is observed at $T = 0.2$, where it moves up further from the hot wall and finally causes the gradient of the temperature to fall. The behavior demonstrates that heat transfer declines with the augmentation of Hartmann number. As Hartmann number increases from Ha = 0 to 25, a new circulation is produced at the bottom of the cavity and the value of the stream function for the main flow decreases.

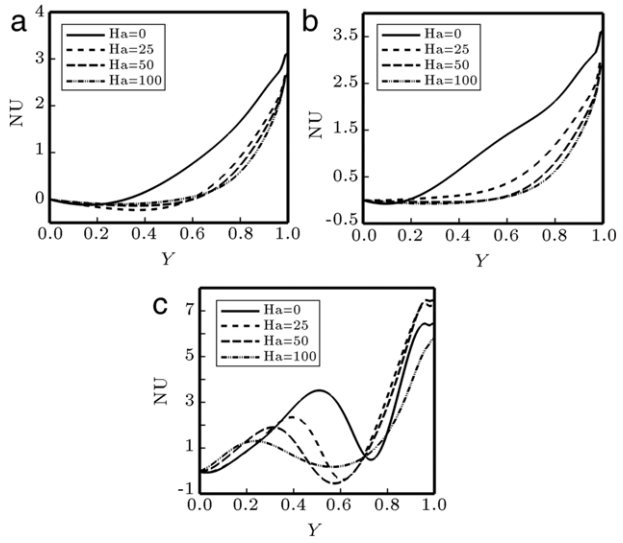

Figure 10: Local Nusselt number distributions on the left wall at various Richardson numbers and Hartman numbers for $\theta = 0^{\circ}$. (a) Ri = 0.01, (b) Ri = 1, and (c) Ri = 100.

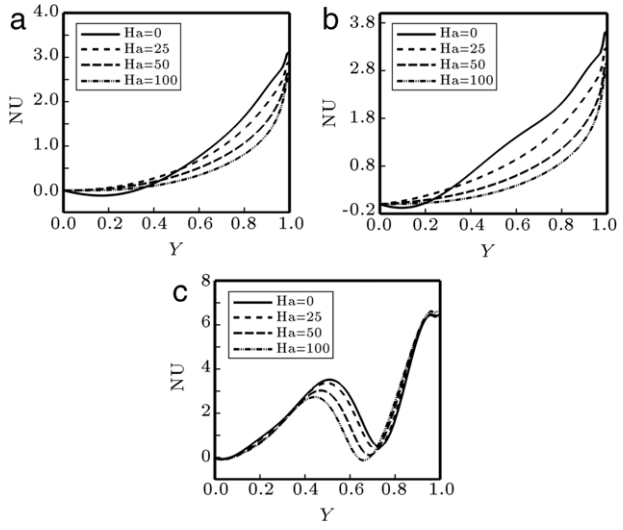

Figure 11: Local Nusselt number distributions on the left wall at various Richardson numbers and Hartman numbers for $\theta = 90^{\circ}$ (a) Ri = 0.01, (b) Ri = 1, (c) Ri = 100.

At Ha = 50, the value of the stream functions continue their declining trend, and a new weak circulation is created, which agrees with the main flow. The second circulation, which circulates counterclockwise in the middle of the cavity, ameliorates, and the main flow at the top of the cavity weakens, whereas the third circulation extends at Ha = 100.

Figure 5 exposes the effect of Hartmann number at Ri = 1. The isotherm has a similar profile with Ri = 0.01 against the increment of Hartmann number. The core of the stream function moves up at Ha = 25 and a vortex is erected by a marked increase in Hartmann number to Ha = 50. But, at Ha = 100, a secondary circulation exists marginally in the middle of the cavity as two main circulations surround it.

In Figure 6, we consider the isotherms and the streamlines for multifarious Hartmann numbers and Ri = 100. The effect of Hartmann number in the isotherms is evident where they rise toward the top wall, and a depletion of the temperature gradient on the hot bottom wall is seen. At Ha = 25, secondary circulation develops and the core of the main flow moves downwards. For high Hartmann numbers, the change in the stream functions is negligible, and exclusively the power of the secondary circulation decreases, and marginal movement at the top of the cavity for the stream function was observed.

Table 1: Grid independence study.

Mesh size	NU_h	Time (s)
25 × 25	1.19	15.953
50 × 50	1.125	23.953
75 × 75	1.146	43.453
100 × 100	1.165	104.875
125 × 125	1.165	356.281

5.4. Effect of Hartmann number on the streamlines and isotherms in a Y-direction magnetic field

Figure 7 illustrates the isotherms and streamlines for three different Hartmann numbers, as Richardson number is fixed at Ri = 0.01. It is obvious that the changes of the isotherms are marginal by the growth of Hartmann number. But, the streamlines exhibit sundry trends for each Hartmann number, whilst the core of the main flow approaches the top wall of the cavity. Meanwhile the value of the stream function drops steadily and the streamlines form linearly in the middle of the cavity by the rise of Hartmann number.

Figure 8 shows the effect of Hartmann number on the streamlines and isotherms at Ri = 1. As can be seen, the counters have a similar pattern, with Ri = 0.01, towards the growth of Hartmann number. With the differences that the streamlines have a downward inclination in the center of the flow field and at Ha = 25, the isotherms have more convection against Ri = 0.01, where $T = 0.3$ draws to the edges of the cavity, conversely at Ri = 0.01.

Figure 9 explores the isotherms and streamlines for various Hartmann numbers at Ri = 100. As Hartmann number soars, the secondary circulation at the corner of the cavity become intense and the circular core of the flow changes to an elliptical form. Hartmann number influences the isotherm noticeably, just at $T = 0.5$, which moves up.

5.5. Effect of magnetic field on Nusselt number

Distribution of the local Nusselt number on the linearly heated wall for various Hartmann and Richardson numbers, as $\theta = 0^{\circ}$, was considered in Figure 10. At Ri = 0.01 and 1, the Nusselt number exhibits a similar manner, decreasing with the augmentation of Hartmann number. A noticeable point at Ri = 0.01 is at $0.2 < y < 0.4$ for Ha = 25, which places it at the lowest point contrary to the impression. Also, the space between Hartmann numbers of 0 and 25 is more at Ri = 0.01. A sinusoidal behavior is observed for distribution of the local Nusselt number at Ri = 100, as it is irregular for various Hartmann numbers, but it is interesting that the maximum and minimum values of Nusselt number occur at Ha = 50.

Figure 11 depicts the local Nusselt number on the left wall, as Hartmann number and Richardson number vary at $\theta = 90^{\circ}$. The local Nusselt number declines gradually by the growth of Hartmann number, except at $0 < y < 0.2$, where Ha = 0 has the lowest value. At Ri = 100, similar to $\theta = 0^{\circ}$, it has a sinusoidal distribution, with this difference, that it behaves

Table 2: Comparison of average Nusselt number with available results in the literature for lid-driven cavity for $Gr = 100$ and $Pr = 0.71$.

Re	Ri	Present work	Waheed [1]	Tiwari and Das [7]	Abdelkhalek [6]	Khanafer et al. [5]	Sharif [4]	Khanafer and Chamka [3]	Iwatsu et al. [2]
1	100	1.0094	1.00033	–	–	–	–	–	–
100	0.01	2.09	2.03116	2.10	1.985	2.02	–	2.01	1.94
400	0.00062	4.08082	4.0246	3.85	3.8785	4.01	4.05	3.91	3.84
1000	0.0001	6.54687	6.48423	6.33	6.345	6.42	6.55	6.33	6.33

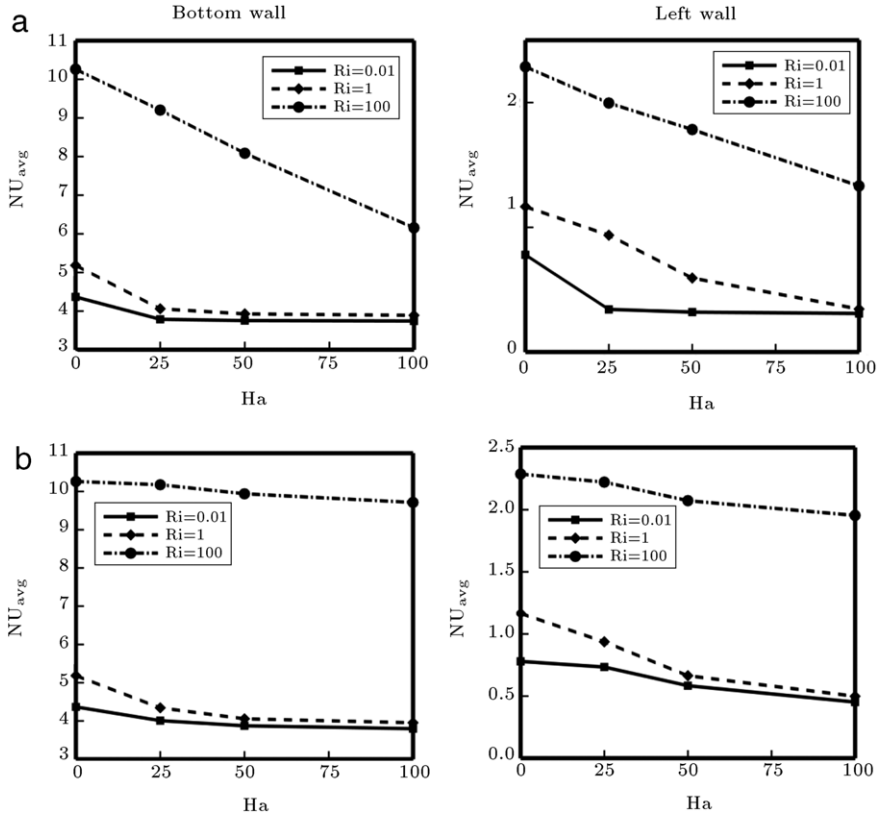

Figure 12: Average Nusselt number distributions on the left wall at various Richardson number for (a) $\theta = 0^\circ$, and (b) $\theta = 90^\circ$.

regularly and steadily, whilst the maximum and minimum values of Nusselt number belong to Ha = 100.

Figure 12 demonstrates the average Nusselt number on the left and the bottom walls for two directions of magnetic field. Generally, the average Nusselt number drops gradually with an increase in Hartmann number at $\theta = 90^\circ$ for two walls, while at $\theta = 0^\circ$, this decline is sharp, and the behavior is more evident at Ri = 100. Meanwhile, it shows that the effect of high Hartmann number is negligible at Ri = 0.01 and 1 for all cases.

6. Conclusion

In this paper, the effects of a magnetic field on mixed convection flow in a lid-driven cavity with a linearly heated wall have been analyzed using the lattice Boltzmann method. In this method, just the force term at LBM changes in the presence of MHD flow, as the added term rises from the classic equations of fluid mechanics. Moreover, all parameters of the added term and the method of their computing are exhibited. This study has been carried out for pertinent parameters in the following ranges: the Richardson number of base fluid, Ri = 0.01 − 100, the Hartmann number of the magnetic field between 0 and 100, and Reynolds number fixed at Re = 100, where the direction of the magnetic field was conducted at $\theta = 0^\circ$ and 90°. This investigation was performed for various mentioned parameters, and some conclusions were summarized as follows:

(a) A good agreement, valid with previous numerical investigations demonstrates that the Lattice Boltzmann Method is an appropriate method for different applicable problems.

(b) Heat transfer is augmented by the growth of Richardson number.

(c) Heat transfer declines with the increment of Hartmann number for various Richardson numbers and the directions of the magnetic field.

(d) At Ri = 0.01 and 1, the effect of the magnetic field is marginal for high Hartmann numbers.

(e) At $\theta = 0^\circ$, heat transfer reduces with augmentation of the Hartmann number higher than $\theta = 90^\circ$ for Ri = 100, but, for Ri = 0.01 and 1, the trend is similar.

(f) At $\theta = 0^\circ$, for high Hartmann number, a secondary circulation is created opposite to the main flow direction, causing heat transfer to decrease.

References

[1] Waheed, M.A. "Mixed convective heat transfer in rectangular enclosures driven by a continuously moving horizontal plate", *Int. J. Heat Mass Transfer*, 52, pp. 5055–5063 (2009).

[2] Iwatsu, R., Hyun, J.M. and Kuwahara, K. "Mixed convection in a driven cavity with a stable vertical temperature gradient", *Int. J. Heat Mass Transfer*, 36, pp. 1601–1608 (1993).

[3] Khanafer, K. and Chamkha, A.J. "Mixed convection flow in a lid-driven enclosure filled with a fluid-saturated porous medium", *Int. J. Heat Mass Transfer*, 42, pp. 2465–2481 (1999).

[4] Sharif, M.A.R. "Laminar mixed convection in shallow inclined driven cavities with hot moving lid on top and cooled from bottom", *Appl. Therm. Eng.*, 27, pp. 1036–1042 (2007).

[5] Khanafer, K.M., Al-Amiri, A.M. and Pop, I. "Numerical simulation of unsteady mixed convection in a driven cavity, using an externally excited sliding lid", *Eur. J. Mech. B/Fluids*, 26, pp. 669–687 (2007).

[6] Abdelkhalek, M.M. "Mixed convection in a square cavity by a perturbation technique", *Comput. Mater. Sci.*, 42, pp. 212–219 (2008).

[7] Tiwari, R.K. and Das, M.K. "Heat transfer augmentation in a two-sided lid-driven differentially heated square cavity utilizing nanofluids", *Int. J. Heat Mass Transfer*, 50, pp. 2002–2018 (2007).

[8] Sivakumar, V., Sivasankaran, S., Prakash, P. and Lee, J. "Effect of heating location and size on mixed convection in lid-driven cavities", *Comput. Math. App.*, 59, pp. 3053–3065 (2010).

[9] Kahveci, K. and Oztuna, S. "MHD natural convection flow and heat transfer in a laterally heated partitioned enclosure", *Eur. J. Mech. B/Fluids*, 28, pp. 744–752 (2009).

[10] Pirmohammadi, M. and Ghassemi, M. "Effect of magnetic field on convection heat transfer inside a tilted square enclosure", *Int. Commun. Heat Mass Transfer*, 36, pp. 776–780 (2009).

[11] Sathiyamoorthy, M. and Chamkha, A. "Effect of magnetic field on natural convection flow in a liquid gallium filled square cavity for linearly heated side wall(s)", *Int. J. Therm. Sci.*, 49, pp. 1856–1865 (2010).

[12] Sivasankaran, S., Malleswaran, A., Lee, J. and Sundar, P. "Hydro-magnetic combined convection in a lid-driven cavity with sinusoidal boundary conditions on both sidewalls", *Int. J. Heat Mass Transfer*, 54, pp. 512–525 (2011).

[13] Rahman, M.M., Parvin, S., Saidur, R. and Rahim, N.A. "Magnetohydrodynamic mixed convection in a horizontal channel with an open cavity", *Int. Commun. Heat Mass Transfer*, 38, pp. 184–193 (2011).

[14] Oztop, H.F., Zhao, Z. and Yu, B. "Conduction-combined forced and natural convection in lid-driven enclosures divided by a vertical solid partition", *Int. Commun. Heat Mass Transfer*, 36, pp. 661–668 (2009).

[15] Oztop, H.F., Al-Salem, K. and Pop, I. "MHD mixed convection in a lid-driven cavity with corner heater", *Int. J. Heat Mass Transfer*, 54, pp. 3494–3504 (2011).

[16] Nasrin, R. and Parvin, S. "Hydromagnetic effect on mixed convection in a lid-driven cavity with sinusoidal corrugated bottom surface", *Int. Commun. Heat Mass Transfer*, 38, pp. 781–789 (2011).

[17] Mehravaran, M. and Kazemzadeh Hannani, S. "Simulation of buoyant bubble motion in viscous flows employing lattice Boltzmann and level set methods", *Scientia Iranica*, 18, pp. 231–240 (2011).

[18] Pirouz, M., Farhadi, M., Sedighi, K., Nemati, H. and Fattahi, E. "Lattice Boltzmann simulation of conjugate heat transfer in a rectangular channel with wall-mounted obstacles", *Scientia Iranica*, 18, pp. 213–221 (2011).

[19] Kefayati, G.H.R., Hosseinizadeh, S.F., Gorji, M. and Sajjadi, H. "Lattice Boltzmann simulation of natural convection in tall enclosures using water/SiO_2 nanofluid", *Int. Commun. Heat Mass Transfer*, 38, pp. 798–805 (2011).

[20] Kefayati, G.H.R., Hosseinizadeh, S.F., Gorji, M. and Sajjadi, H. "Lattice Boltzmann simulation of natural convection in an open enclosure subjugated to water/copper nanofluid", *Int. J. Therm. Sci.*, 52, pp. 91–101 (2011).

[21] Sajjadi, H., Hosseinizadeh, S.F., Gorji, M., Kefayati, G.H.R. and Ganji, D.D. "Numerical analysis of turbulent natural convection in square cavity using large-eddy simulation in Lattice Boltzmann method", *Iran. J. Sci. Tech.*, 35, pp. 133–142 (2011).

Gholamreza Kefayati received his B.S. degree from the School of Mechanical Engineering, Thermo-fluids, at the Islamic Azad University, Tehran South Branch, and his M.S. degree in Energy Conversion from the School of Mechanical Engineering at Babol University of Technology, Iran. His main research interests include computational fluid dynamics and nanofluids, MHD & multiphase flows utilizing LBM.

Mofid Gorji-Bandpy received his Ph.D. degree in Mechanical Engineering from the University of Wales, Cardiff, UK, and is now Professor of Mechanical Engineering at Babol Noshirvani University of Technology, Iran. His research work concerns: fluid mechanics, turbomachinery and all hydro-engineering subjects, renewable energy, water distribution networks, mechanics and thermodynamics of propulsion systems and internal combustion chamber.

Hasan Sajjadi is a Ph.D. degree student of Mechanical Engineering at Shahid Bahonar University of Kerman. He received his M.S. degree from Babol University of Technology, Iran, in 2011, and his Licentiate degree from Isfahan University of Technology, Iran, in 2009. His main research areas include: turbulence modeling (LES) using lattice Boltzmann method, nonlinear science in engineering & computational fluid dynamics.

Davood Domiri Ganji received his Ph.D. degree in Mechanical Engineering from Tarbiat Modaress University, Iran, and is now Associate Professor of Mechanical Engineering at Babol Noshirvani University of Technology, Babol, Iran. His research interests include nonlinear science in engineering, CFD, inverse problems and spray modeling.